

Stability Diagram and Critical Time Delay for the Kuramoto Model with Heterogeneous Interaction Delays*

Per Sebastian Skardal

Department of Mathematics, Trinity College, Hartford, CT 06106, USA

Abstract

We present a bifurcation analysis for the Kuramoto model of coupled oscillators with heterogeneous interaction delays. Following the groundbreaking dimensionality reduction of Ott and Antonsen [E. Ott and T. M. Antonsen, *Chaos* **18**, 037113 (2008)], Lee et al. [W. S. Lee, E. Ott, and T. M. Antonsen, *Phys. Rev. Lett.* **103**, 044101 (2009)] showed that the dynamics of time delayed coupled oscillator systems could be similarly reduced by considering heterogeneous delays, confirming the presence of multistability between incoherence and partial synchronization. Here we study the series of bifurcations in the system and describe the full stability diagram for the macroscopic system dynamics. The transition from incoherence to partial synchronization comes in one of two forms: (i) via a supercritical Hopf bifurcation, in which case no multistability exists, or (ii) via a subcritical Hopf bifurcation with a saddle node bifurcation of cycles, in which case the incoherent and partially synchronized states are both stable for a range of coupling strengths. The transition between these two combinations of bifurcations occurs at a codimension two point, which can be expressed analytically and allows us to identify a critical characteristic time delay below which no multistability can emerge in the system dynamics.

1 Introduction

1.1 Background

The dynamics of large systems of coupled oscillators represent an important area of study in nonlinear science due to their utility in modeling a wide variety of natural and engineered phenomena [1, 2]. Examples include rhythmic flashing of fireflies [3], circadian rhythms [4], cardiac pacemakers [5], and synchronization in power grids [6]. The Kuramoto model, which was designed as an analytically tractable alternative to Winfree’s seminal model [7], is a particularly important example where oscillators are each defined by a single phase angle with its own natural frequency and are globally coupled through a sinusoidal coupling function [8]. Since its genesis, researchers in the nonlinear sciences have thoroughly studied the dynamics of further extensions of the Kuramoto model, for example external noise [9, 10] and bimodal frequency distributions [11, 12].

* Abbreviated Title: Stability Diagram for the Time Delayed Kuramoto Model

A particularly important extension of the Kuramoto model involves the incorporation of time delays in the interactions between oscillators. The equations of motion for the time delayed Kuramoto model are given by

$$\dot{\theta}_i = \omega_i + \frac{K}{N} \sum_{j=1}^N \sin[\theta_j(t - \tau_{ij}) - \theta_i(t)], \quad (1)$$

where θ_i represents the phase angle of oscillator i , where $i = 1, \dots, N$ and the system consists of N oscillators, ω_i is the natural frequency of oscillator i , which we assume is drawn from a distribution $g(\omega)$, $K \geq 0$ is the global coupling strength, and $\tau_{ij} \geq 0$ represents the interaction delay between oscillators i and j . The degree of synchronization is measured by the magnitude of the complex order parameter

$$z = r e^{i\psi} = \frac{1}{N} \sum_{j=1}^N e^{i\theta_j} \quad (2)$$

where $r \approx 0$ and $r \sim 1$ correspond to incoherent and partially synchronized states, respectively. Early investigations into the dynamics of Eq. (1) focused on the case of a single time delay (i.e., $\tau_{ij} = \tau$ for all i, j) and observed the emergence of multistability between incoherence and partial synchronization, a novel dynamical property which is absent in the classical Kuramoto model without time delays [13, 14, 15, 16]. However, further analytical progress characterizing the macroscopic dynamics remained elusive, leaving several questions unanswered. For instance, where and how do bifurcations occur? What does the general stability diagram look like? Depending on the other system parameters, at what characteristic time delay does multistability emerge? Given a positive characteristic time delay, is it always possible to observe multistability, or is there a critical characteristic time delay below which multistability cannot be observed?

In 2008 Ott and Antonsen [17, 18] discovered a remarkable technique for reducing the dimensionality of large oscillator systems, thereby facilitating breakthroughs in the analytical descriptions in a wide variety of Kuramoto model extensions. Examples where their technique was applied include systems with external forcing [19], bimodal frequency distributions [20, 21], community structure [22, 23, 24], assortative and disassortative network structures [25, 26], pulse-coupled oscillations [27, 28, 29], positive and negative coupling strengths [30], and high-order coupling [31]. In Ref. [32] Lee et al. demonstrated that the technique could be applied to the time delay case by allowing for delays to be heterogeneously distributed according to certain classes of a delay distribution $h(\tau)$. These results put on firmer ground the existence of multistability for certain parameter choices and were used to explore the dynamics of further extensions of the model, including the spatially extended case [33, 34] and adaptive coupling [35]. However, a unified bifurcation analysis remains lacking, specifically an analytical description of its bifurcations for general parameters, leading to a full stability diagram, as well as an analysis of the emergence of multistability and a critical characteristic time delay.

1.2 Preliminaries

Before proceeding with our analysis we introduce a few more important properties of the system. In the classical Kuramoto model without time delays the analysis is facilitated by the fact that the

equations of motion can be rewritten using the order parameter. To this end, we use the collection of time delayed order parameters [32] which are defined as

$$w_i = \rho_i e^{i\phi_i} = \frac{1}{N} \sum_{j=1}^N e^{i\theta_j(t-\tau_{ij})}, \quad (3)$$

which represents a similar mean-filed order parameter as the order parameter in Eq. (2), but delayed according to the time delays τ_{ij} associated with oscillator i . Using this collection of time delayed order parameters, Eq. (1) can be rewritten as

$$\dot{\theta}_i = \omega_i + \frac{K}{2i} \left(w_i e^{-i\theta_i} - w_i^* e^{i\theta_i} \right) = \omega_i + K\rho_i \sin(\phi_i - \theta_i), \quad (4)$$

where $*$ represents the complex conjugate.

Next we describe our choices of distributions for the time delays and natural frequencies. As noted above, we consider the case of heterogeneous time delays. Specifically, we assume that the distribution h is exponential, i.e.,

$$h(\tau) = \begin{cases} e^{-\tau/T}/T & \text{if } \tau \geq 0, \\ 0 & \text{if } \tau < 0, \end{cases} \quad (5)$$

where the parameter $T \geq 0$ represents the characteristic time scale and mean for the interaction delays. In Ref. [32] Lee et al. considered the family of general Gamma distributions, i.e., the natural generalization of Eq. (5), which we comment on later. For purposes of obtaining analytical results we will also restrict our attention to the case of a Lorentzian frequency distribution of the form

$$g(\omega) = \frac{\Delta}{\pi [\Delta^2 + (\omega - \omega_0)^2]}, \quad (6)$$

where $\Delta > 0$ represents the characteristic width of the distribution and ω_0 represents the mean natural frequency of the system.

In the remainder of this paper we analyze the dynamics of Eq.(1) for these choices. In Sec. 2 we summarize the dimensionality reduction for the system first described in Refs. [17, 32] and discuss the physical interpretations for the reduced dynamics. In Sec. 3 we present the main contributions of this work, describing the bifurcations that occur in the system, building the stability diagram, and investigate the critical time delay. In particular, we describe a series of Hopf bifurcations, both supercritical and subcritical, and a saddle node bifurcation of cycles that partition the stability diagram into distinct regions. Importantly, we show that multistability emerges as the supercritical Hopf bifurcations gives way to a subcritical Hopf bifurcation and a saddle node bifurcation of cycles emerges, forming a hysteresis loop. The emergence of this hysteresis loop occurs at a codimension two point where the saddle node bifurcation collides with the Hopf bifurcations. Moreover, by characterizing this codimension two point we determine a non-zero critical characteristic time delay exists: only above this critical characteristic time delay can the system achieve multistability. Finally, we revisit the Hopf bifurcation with a stability analysis for the incoherent state. In Sec. 4 we conclude with a discussion of our results.

2 Dimensionality Reduction

Following the technique presented in Refs. [17, 32], we consider the system whose dynamics are governed by Eq. (1) in the limit of $N \rightarrow \infty$ oscillators. In this scenario, we may describe the macroscopic state of the system using the distribution function $f(\theta, \omega, t)$, such that $f(\theta, \omega, t)d\theta d\omega$ describes the fraction of oscillators with phases between θ and $\theta + d\theta$ and frequencies between ω and $\omega + d\omega$ at time t . In this continuum limit we may rewrite the instantaneous order parameter as

$$z(t) = \int_{-\infty}^{\infty} \int_0^{2\pi} f(\theta, \omega, t) e^{i\theta(t)} d\theta d\omega. \quad (7)$$

Since the time delays τ_{ij} are all drawn from the same distribution, we have that in this limit the time delayed order parameters are all equivalent, i.e., $w_i(t) = w(t)$ for all i , and can be written

$$w(t) = \int_0^{\infty} z(t - \tau) h(\tau) d\tau. \quad (8)$$

Moreover, the conservation of oscillators implies that the distribution function f satisfies the following continuity equation:

$$0 = \frac{\partial}{\partial t} f + \frac{\partial}{\partial \theta} (f \dot{\theta}) = \frac{\partial}{\partial t} f + \frac{\partial}{\partial \theta} \left\{ f \left[\omega + \frac{K}{2i} (we^{-i\theta} - w^* e^{i\theta}) \right] \right\}. \quad (9)$$

Finally, because f lives on the circle in the θ dimension it is natural to expand it into its Fourier series, which must be of the form

$$f(\theta, \omega, t) = \frac{g(\omega)}{2\pi} \left\{ 1 + \sum_{n=1}^{\infty} \left[f_n(\omega, t) e^{in\theta} + f_n^*(\omega, t) e^{-in\theta} \right] \right\}. \quad (10)$$

The dimensionality reduction discovered by Ott and Antonsen [17] consists of an ansatz for the sequence of the Fourier coefficients in Eq. (10), specifically that they decay geometrically, i.e., $f_n(\omega, t) = a^n(\omega, t)$. Remarkably, inserting this ansatz into Eq. (10) then Eq. (9) reduces the partial differential equations in Eq. (9) to an ordinary differential equation for a of the form

$$0 = \frac{\partial a}{\partial t} + i\omega a + \frac{K}{2} (wa^2 - w^*). \quad (11)$$

Moreover the dynamics defined for the function $a(\omega, t)$ in Eq. (11) can be connected back to those of the instantaneous order parameter by inserting the Fourier series into Eq. (7), which yields

$$z(t) = \int_{-\infty}^{\infty} g(\omega) a^*(\omega, t) d\omega. \quad (12)$$

Recall now that we assumed a Lorentzian frequency distribution g , which can be rewritten

$$g(\omega) = \frac{\Delta}{\pi [\Delta^2 + (\omega - \omega_0)^2]} = \frac{1}{2\pi i} \left(\frac{1}{\omega - \omega_0 - i\Delta} - \frac{1}{\omega - \omega_0 + i\Delta} \right), \quad (13)$$

Using Eq. (13), the integral in Eq. (12) can be evaluated by closing the contour in the bottom-half ω complex plane containing the pole $\omega = \omega_0 - i\Delta$, yielding $z(t) = a^*(\omega_0 - i\Delta, t)$. (See Ref. [17].) Finally, taking a complex conjugate of Eq. (11), evaluating at $\omega = \omega_0 - i\Delta$, and rearranging yields

$$\dot{z} = -\Delta z + i\omega_0 z + \frac{K}{2} (w - w^* z^2). \quad (14)$$

In principle, Eq. (14) closes the dynamics of the system along with Eq. (8). However, for a bifurcation analysis it is convenient to convert the integral in Eq. (8) into a differential equation. In Ref. [32] Lee et al. show that this is possible using a Laplace transform. In particular, Eq. (8) is a convolution, and therefore its Laplace transform is given by

$$\hat{w}(s) = \hat{z}(s)\hat{h}(s), \quad (15)$$

where $\hat{\cdot}$ represents the Laplace transform. Since h is exponential, i.e., $h(\tau) = e^{\tau/T}/T$, we have that

$$\hat{h}(s) = \frac{1}{1 + Ts} \rightarrow (1 + Ts)\hat{w}(s) = \hat{z}(s). \quad (16)$$

We then convert back to the time domain and rearrange to obtain

$$T\dot{w} = z - w, \quad (17)$$

thus closing the dynamics of the system with Eqs. (14) and (17).

Before proceeding with a bifurcation analysis, we briefly discuss the physical interpretation of Eqs. (14) and (17). Equation (14) states that the dynamics of the instantaneous order parameter z evolves nonlinearly in response to the state of the time delayed order parameter w . Equation (17), on the other hand, states that the time delayed order parameter w “chases” the instantaneous order parameter with a natural time scale T , given by the mean of the original distribution of time delays. In the limit $T \rightarrow 0^+$ the time delays vanish and $w = z$, corresponding to the classical Kuramoto model where each τ_{ij} in Eq. (1) vanishes. On the other hand, for large T the dynamics of w follow more slowly behind those of z , which impede the synchronization of the system as we will see below.

3 Bifurcation Analysis

3.1 Scaling

We begin our analysis of the reduced dynamics in Eqs. (14) and (17) with a rescaling to reduce the number of system parameters. In particular, we eliminate the parameter Δ by first defining

$$\tilde{t} = \Delta t, \quad (18)$$

$$\tilde{K} = K/\Delta, \quad (19)$$

$$\tilde{\omega}_0 = \omega_0/\Delta, \quad (20)$$

$$\tilde{T} = \Delta T, \quad (21)$$

and then dividing Eqs. (14) and (17) by Δ , obtaining

$$\dot{z} = -z + i\omega_0 z + \frac{K}{2} (w - w^* z^2), \quad (22)$$

$$T\dot{w} = z - w, \quad (23)$$

where the overdot now corresponds to differentiation with respect to rescaled time and we have dropped the \sim for notational simplicity. This rescaling eliminates the parameter Δ by effectively fixing the width of the frequency distribution $g(\omega)$ to one with the remaining parameters appropriately rescaled. This rescaling essentially speeds up time, reduces the coupling strength and mean of the frequency distribution, and stretches the time delay distribution, all by a factor of the original value of Δ .

3.2 Steady-state dynamics and the $T = 1$ case

We now study the dynamics of the rescaled Eqs. (22) and (23). For this purpose, it is convenient to convert to polar coordinates, i.e.,

$$\dot{r} = -\Delta r + \frac{K}{2}\rho(1-r^2)\cos(\phi-\psi), \quad (24)$$

$$\dot{\psi} = \omega_0 + \frac{K}{2}\rho\frac{1+r^2}{r}\sin(\phi-\psi), \quad (25)$$

$$T\dot{\rho} = r\cos(\phi-\psi) - \rho, \quad (26)$$

$$T\dot{\phi} = -\frac{r}{\rho}\sin(\phi-\psi). \quad (27)$$

We note that Eqs. (24)–(27) display a rotational invariance of the form $\psi \mapsto \psi + \delta$ and $\phi \mapsto \phi + \delta$, suggesting the existence of rotationally symmetric solutions. These solutions can be found by searching for steady-state behavior with fixed amplitudes and angular velocities, i.e., setting $\dot{r} = \dot{\rho} = 0$ and $\dot{\psi} = \dot{\phi} = \Omega$, where Ω represents the angular velocity. Inserting this into Equations (22) and (23) and using that $\cos^2 x + \sin^2 x = 1$ yields

$$\rho = \frac{r}{\sqrt{1+T^2\Omega^2}}. \quad (28)$$

This can in turn be inserted into Eqs. (24) and (25) to yield a system of nonlinear equations that implicitly determines the steady-state values of r and Ω :

$$r = \frac{K}{2} \frac{r(1-r^2)}{1+T^2\Omega^2}, \quad (29)$$

$$\Omega = \omega_0 - \frac{K}{2}(1+r^2) \frac{T\Omega}{1+T^2\Omega^2}. \quad (30)$$

Inspecting Eqs. (29) and (30), the incoherent state $r = 0$ is always a trivial solution (in which case the angular velocity Ω has no meaning). Below we will present a stability analysis of the incoherent solution. Nontrivial solutions $r > 0$ that correspond to partial synchronization are in general more difficult to find analytically. We note also that moving forward we will consider cases where the mean natural frequency is positive, $\omega_0 > 0$, in which case it is also reasonable to search for solutions with a positive angular velocity, $\Omega > 0$. (The analysis for $\omega_0 < 0$ runs similarly, in which case $\Omega < 0$.)

To shed light on the nature of nontrivial solutions it is useful to consider the case $T = 1$, in which case analytical expressions for r and Ω can be written down explicitly. Setting $T = 1$ and ignoring the incoherent state, we solve for r in Eq. (29), which we insert into Eq. (30) and rearrange to find

$$\Omega = \frac{K \mp \sqrt{K^2 - 4\omega_0^2}}{2\omega_0}. \quad (31)$$

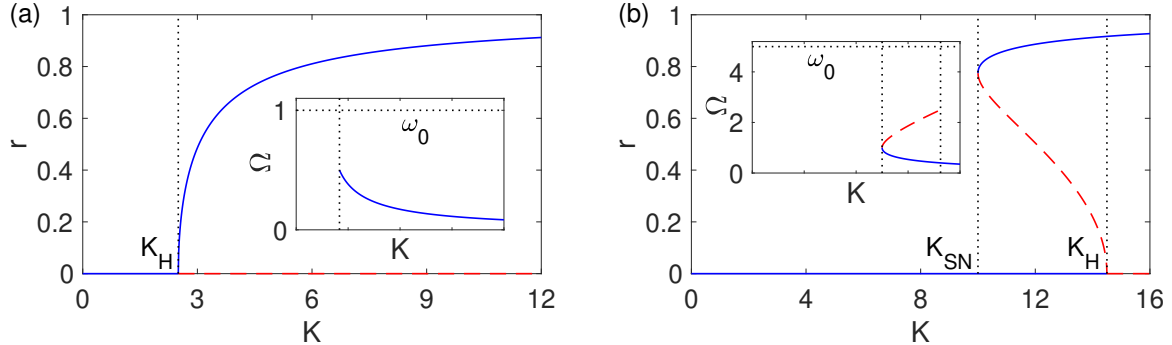


Figure 1: *Transitions to partial synchronization for $T = 1$: super and subcriticality.* Steady-state solutions of r vs K with $T = 1$ for (a) $\omega_0 = 1$ and (b) 5, as examples of, respectively, a typical transition to partial synchronization through a supercritical Hopf bifurcation and via a hysteresis loop with a saddle node bifurcation of cycles and subcritical Hopf bifurcation. Stable and unstable branches are illustrated in solid blue and dashed red, respectively. Insets: steady-state solutions for the angular velocity Ω corresponding to partially synchronized solutions.

Inserting this back into Eq. (29) and neglecting the incoherent state yields

$$r = \frac{\sqrt{\omega_0^2 - K \pm \sqrt{K^2 - 4\omega_0^2}}}{\omega_0}, \quad (32)$$

where we have also neglected the two negative solutions of r . We emphasize that the steady-state values of r given in Eq. (32) do not correspond to fixed points, but rather limit cycles with fixed amplitude r and angular velocity Ω . Inspecting Eq. (32) more closely, the inner-most square root implies that a nontrivial solution for r exists only if $K \geq 2\omega_0$. Beyond this coupling strength, the solution in Eq. (32) corresponding to the positive sign always exists, while the outer-most square root implies that the solution corresponding to the negative sign exists only if $K \geq (\omega_0^2 + 4)/2$.

In Figs. 1(a) and (b) we plot the solutions in Eq. (32) for $\omega_0 = 1$ and 5, respectively. Branches that are stable and unstable are plotted in solid blue and dashed red, respectively. For sufficiently small ω_0 , e.g., $\omega_0 = 1$, we see that the transition from incoherence to partial synchronization is typical in the sense that it is qualitatively similar to the transition in the classical Kuramoto model: a second-order phase transition from incoherence to partial synchronization owing to a supercritical Hopf bifurcation that occurs at a critical value we denote $K = K_H$. However, for larger ω_0 , e.g., $\omega_0 = 5$, this transition folds onto itself into a hysteresis loop as a saddle node bifurcation of cycles emerges at $K = K_{SN} < K_H$ and the Hopf bifurcation becomes subcritical. For the case of $T = 1$ these critical bifurcation values can be characterized by the values for which the solutions in Eq. (32) appear and annihilate. Specifically, the Hopf bifurcation occurs at $K_H = (\omega_0^2 + 4)/2$ and the saddle-node bifurcation of cycles occurs at $K_{SN} = 2\omega_0$. Moreover, the saddle-node bifurcation of cycles emerges only if ω_0 is large enough, i.e., larger than the intersection between K_H and K_{SN} which occurs at $\omega_0 = 2$. For the time being we forgo discussing the stability properties of these solutions, but will revisit this question below with a closer analysis of the Hopf bifurcation.

3.3 Hopf and saddle node bifurcations

Next we seek to characterize the Hopf and saddle node of cycles bifurcations illustrated for the $T = 1$ case, but for other values of T . (In this portion of the analysis we will not address any stability properties, but will do so below.) Specifically, we search for the critical coupling values K_H and K_{SN} at which these bifurcations occur. We begin with the Hopf bifurcation, which occurs when the partially synchronized solution $r > 0$ collides with the incoherent solution $r = 0$. To find this point we eliminate the incoherent solution from Eq. (29), evaluate the limit $r \rightarrow 0^+$, insert this into Eq. (30), take the limit $r \rightarrow 0^+$ again, and solve for Ω to obtain

$$\Omega = \frac{\omega_0}{1+T}. \quad (33)$$

Inserting Eq. (33) back into Eq. (29) (still in the $r \rightarrow 0^+$ limit) and rearranging, we have that the Hopf bifurcation occurs at

$$K_H = 2 + \frac{2T^2\omega_0^2}{(1+T)^2}. \quad (34)$$

Moving now to the saddle node bifurcation of cycles, we note that K_{SN} coincides with a folding of both r and Ω where $0 = dK/dr = dK/d\Omega$. Choosing to work with $dK/d\Omega$ for simplicity, we eliminate the incoherent solution and solve for r in Eq. (29), which we insert into Eq. (30) and rearrange to obtain

$$K = \frac{(\omega_0 - \Omega + T\Omega)(1 + T^2\Omega^2)}{T\Omega}. \quad (35)$$

We then impose the constraint $dK/d\Omega = 0$, which yields the expression (after multiplying by $T\Omega^2$ for convenience)

$$2T^2(T-1)\Omega^3 + \omega_0T^2\Omega^2 - \omega_0 = 0. \quad (36)$$

The bifurcation point K_{SN} is then obtained by solving Eq. (36) for Ω and inserting this back into Eq. (35), however a few remarks are in order regarding this procedure. First, the left hand side of Eq. (35) is cubic and thus it may have one or more roots that are difficult to express analytically; in practice we find it best to solve numerically. Second, the nature of these solutions depends on the characteristic time delay T . Recall that $\omega_0 > 0$ and we search for a positive solution, $\Omega > 0$. Note then that at $\Omega = 0$ the left hand side of Eq. (36) is negative, so that if $T \geq 1$ only one such positive solution exists since the derivative of the left hand side is positive for all $\Omega > 0$. However, for $T < 1$ another, larger, positive solution arises provided that ω_0 is large enough. Of these two roots we choose the smaller, which corresponds to the single positive root that exists for $T \geq 1$. Finally, this solution is only valid if the corresponding solution for r is real (and non-negative). To check this, we eliminate the incoherent solutions from Eq. (29) and solve for r , yielding

$$r = \sqrt{1 - \frac{2(1 + T^2\Omega^2)}{K}}. \quad (37)$$

Thus, the saddle node bifurcation of cycles exists only if the solution to Eqs. (35) and (36) satisfies

$$\frac{K}{2} \geq 1 + T^2\Omega^2. \quad (38)$$

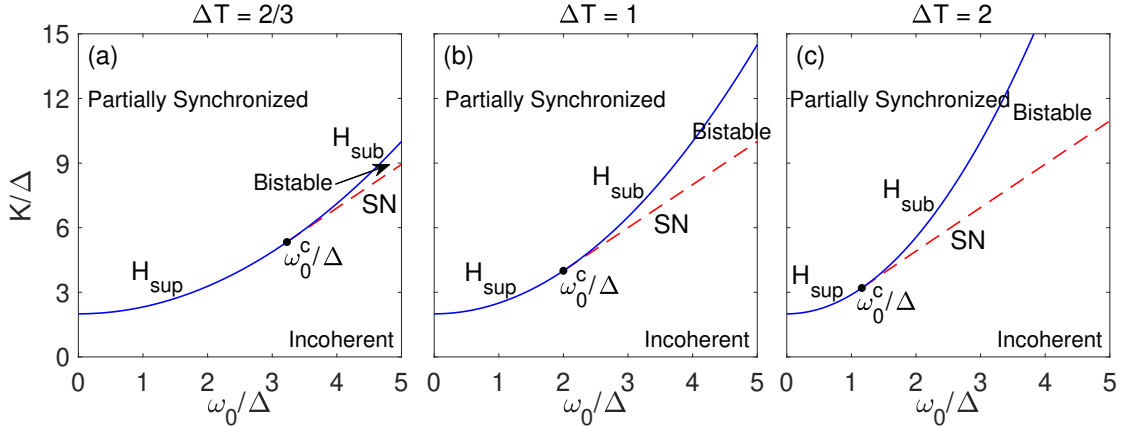


Figure 2: *Stability diagrams*. Stability diagrams in $(\omega_0/\Delta, K/\Delta)$ parameter space for (a) $\Delta T = 2/3$, (b) $\Delta T = 1$, and (c) $\Delta T = 2$. Solid blue curves denote Hopf bifurcations, labeled H_{sup} and H_{sub} for the supercritical and subcritical cases, respectively, and dashed red curves denote saddle node bifurcations of cycles, labeled SN . These bifurcation curves partition the space into incoherent, partially synchronized, and bistable regions. The saddle node bifurcation collides with the Hopf bifurcations at a codimension two point labeled ω_0^c .

In Figs. 2(a), (b), and (c) we illustrate the stability diagram for the system in terms of the parameter space $(\omega_0/\Delta, K/\Delta)$ for $T = 2/3$, $T = 1$, and $T = 2$, respectively, using the non-scaled parameters of the original system. Hopf bifurcation curves are plotted in solid blue and labeled H_{sup} and H_{sub} for the supercritical and subcritical cases, respectively, and the saddle node bifurcation of cycles curve is plotted in dashed red and labeled SN . These bifurcation curves indicate the transitions between regions of parameter space corresponding to incoherence, partial synchronization, and bistability, where the bistable region is given by the wedge in between the subcritical Hopf and saddle node curves. The bistable state vanishes when these curves collide in a codimension two point denoted with a filled black circle and labeled ω_0^c . We study the behavior of this codimension two point in the following section. We note that, in general, as T increases the bistable region grows, owing to the codimension two point moving in towards a smaller value of ω_0 . Physically, this can be interpreted as larger time delays promoting bistability in the system. Moreover, as ω_0 increases, so do both K_H and K_{SN} , indicating that a larger mean natural frequency inhibits the onset of synchronization.

3.4 Codimension two point and the emergence of hysteresis

In addition to investigating the series of bifurcations for the macroscopic dynamics and the general layout of the stability diagram, we set out to answer two additional questions. First, at what point does multistability emerge? Second, for a given characteristic time delay, is it always possible to observe multistability, or is there a critical characteristic time delay below which multistability cannot be observed? Here we answer these questions by studying the behavior of the codimension two point ω_0^c depicted in the stability diagrams. Recall that ω_0^c occurs at the intersection of the Hopf and saddle node bifurcations. Thus, ω_0^c is precisely the point at which multistability emerges: a hysteresis loop exists for all $\omega_0 > \omega_0^c$, but not for $\omega_0 < \omega_0^c$. Moreover, the existence of ω_0^c indicates the potential for hysteresis for a given time delay T ; specifically, for a given value of T , if ω_0^c

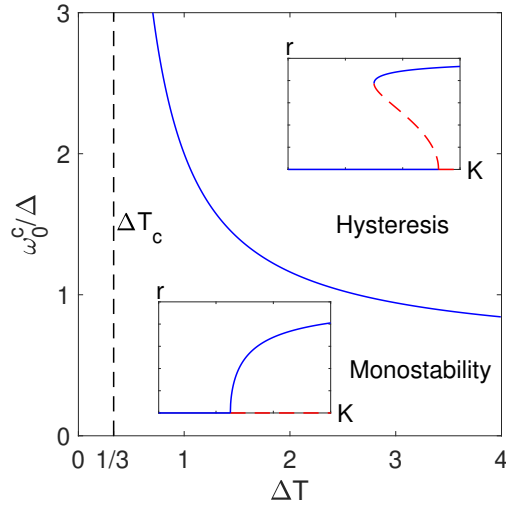


Figure 3: *Codimension two point and the emergence of hysteresis.* Behavior of the codimension two point ω_0^c/Δ denoting the onset of hysteresis as the characteristic time delay ΔT varies. For $\omega_0 < \omega_0^c$ and $\omega_0 > \omega_0^c$ the transition to partial synchronization exhibits monostability and hysteresis, respectively, as illustrated by the insets. Below the critical time delay of $\Delta T_c = 1/3$ no hysteresis is attainable for any values of ω_0 .

exists, then multistability is attainable. However, and if ω_0^c does not exist for this value of T , then multistability cannot be observed for any combination of other system parameters.

Recall now that the codimension two point ω_0^c is given by the point at which the saddle node bifurcation of cycles K_{SN} which is a solution of Eq. (35) and (36) intersects with the Hopf bifurcation K_H given in Eq. (34). Despite the fact that K_{SN} is given implicitly above we show now that the ω_0^c can be explicitly solved for. We begin by noting that the collision of the saddle node bifurcation with the Hopf bifurcation must occur in the limit $r \rightarrow 0^+$. We thus eliminate the incoherent solution from Eq. (29), solve for K , and insert this into the left hand side of Eq. (35), yielding

$$2 = \frac{\omega_0 + T\Omega - \Omega}{T\Omega}. \quad (39)$$

Equation (39) is solved by $\Omega = \frac{\omega_0}{T+1}$, which can then be inserted into Eq. (36) and rearranged to find the codimension two point given by

$$\omega_0^c = \frac{(T+1)^{3/2}}{T\sqrt{3T-1}}, \quad (40)$$

where we have taken the positive root.

The value of ω_0^c given in Eq. (40) corresponds to the onset of hysteresis. The system is monostable (i.e., no bistability exists) if $\omega_0 < \omega_0^c$. At $\omega_0 = \omega_0^c$ the saddle node bifurcation of cycles is born and the Hopf bifurcation goes from supercritical to subcritical, resulting in a hysteresis loop for $\omega_0 > \omega_0^c$. This is illustrated in Fig. 3, where we plot ω_0^c/Δ as a function of ΔT again using the non-scaled parameters of the original system. Below and above this curve we illustrate the transition to synchronization (i.e., a supercritical Hopf and a subcritical Hopf with a saddle node of cycles, respectively). Moreover, Fig. 3 illustrates another important implication from Eq. (40)

namely, the codimension two point ω_0^c does not exist for all values of the time delay parameter T . Specifically, if $T \leq 1/3$ then Eq. (40) admits no real solution for ω_0^c due to the square root in the denominator vanishing or become complex. Moreover, in the limit $T \rightarrow= 1/3^+$ the codimension two point ω_0^c diverges, signifying that as T approaches the critical values of $T_c = 1/3$ from above, a larger mean frequency ω_0 is required to realize hysteresis in the system. Thus, there exists a critical characteristic time delay of $T = 1/3$ below which multistability cannot be observed for any combination of other system parameters, but above this value multistability can be observed, provided that ω_0 is sufficiently large. Moreover, in the limit of large T we have that $\omega_0^c \rightarrow 1/\sqrt{3}$, indicating that the mean natural frequency ω_0 must be larger than this value to observe multistability, even for an arbitrarily large characteristic time delay. Another physical interpretation of Fig. 3 is that the mean natural frequency ω_0 and the characteristic time delay T need to be collectively large enough for bistability to emerge in the system.

3.5 Hopf bifurcation revisited: stability of the incoherent state

In the last portion of our analysis, we revisit the Hopf bifurcation discussed above by studying the stability of the incoherent state $z = w = 0$. Since the polar decompositions $z = re^{i\psi}$ and $w = \rho e^{i\phi}$ are singular around the incoherent state (the phase angles ψ and ϕ lose meaning at this point) we instead study the dynamics of x , y , u , and v where $z = x + iy$ and $w = u + iv$. In this four dimensional state space, the linear stability of the incoherent state is governed by the eigenvalues of the Jacobian DF evaluated at $x = y = u = v = 0$, which is given by

$$DF = \begin{bmatrix} -1 & -\omega_0 & \frac{K}{2} & 0 \\ \omega_0 & -1 & 0 & \frac{K}{2} \\ \frac{1}{T} & 0 & -\frac{1}{T} & 0 \\ 0 & \frac{1}{T} & 0 & -\frac{1}{T} \end{bmatrix}. \quad (41)$$

The incoherent state is stable if all eigenvalues have negative real part, so we search for the critical value of K where the eigenvalues of DF with largest real part are purely imaginary. Moreover, our analysis above suggests that the change in stability occurs in the form of a Hopf bifurcation, where a pair of complex conjugate eigenvalues simultaneously crosses the imaginary axis. In general, the eigenvalues of DF in Eq. (41) are difficult to write down explicitly, so we study them in cases below.

We first consider, as we did above, the simplifying case of $T = 1$, in which case the eigenvalues can in fact be written down explicitly:

$$\lambda = -1 \pm \sqrt{K - \omega_0^2 \pm \sqrt{\omega_0^4 - 2K\omega_0^2}} / \sqrt{2}, \quad (42)$$

where the four different combinations of \pm correspond to the four different eigenvalues of DF . For real, non-negative values of K and ω_0 , the real part of all four eigenvalues in Eq. (42) is $\lambda_{\text{real}} = -1$ provided that $K \leq \omega_0^2/2$. Beyond this value, the eigenvalues with largest real part are given by choosing the plus sign outside of both square roots in Eq. (42). We then identify a Hopf bifurcation by searching for eigenvalues of the form $\lambda = \pm i\lambda_{\text{imag}}$, yielding the constraint

$$\pm i\lambda_{\text{imag}} = -1 + \sqrt{K - \omega_0^2 \pm \sqrt{\omega_0^4 - 2K\omega_0^2}} / \sqrt{2}. \quad (43)$$

Note that for fixed ω_0 , Eq. (43) has two real unknowns, K and λ_{imag} , and two equations (for the plus and minus signs), which are solved by $\lambda_{\text{imag}} = \omega_0/2$ and

$$K_H = \frac{\omega_0^2 + 4}{2}, \quad (44)$$

giving the bifurcation value that matches our analysis for the $T = 1$ case above.

For more general values of T the analysis becomes more cumbersome. For starters, eigenvalues are more difficult to write down explicitly, so it is more convenient to work with the characteristic polynomial of DF , which is given by

$$\frac{[k - 2(1 + \lambda)(1 + \lambda T)]^2 + 4\omega_0^2(1 + \lambda T)^2}{4T^2} = 0. \quad (45)$$

To check that a Hopf bifurcation occurs at the value $K = K_H$ as given in Eq. (34), we search a pair of purely imaginary, conjugate eigenvalues $\lambda = 0 + i\lambda_{\text{imag}}$ that solve Eq. (45). From our analysis above we also found that at the Hopf bifurcation the angular velocity was given by Ω given in Eq. (33). It can then be easily checked that choosing $\lambda = \pm i\Omega$ from Eq. (33) and $K = K_H$ from Eq. (34) solves Eq. (45). Moreover, we have checked numerically that the other two eigenvalues have negative real part, confirming the existence of a Hopf bifurcation at the value $K = K_H$ from Eq. (34).

4 Discussion

In this paper we have studied the macroscopic system dynamics of the Kuramoto model of coupled oscillators with heterogeneous interaction delays. The effects of time delays on the Kuramoto model have been previously investigated [13, 14, 15, 16], most notably giving rise to the possibility of multistability between incoherence and partial synchronization. Recently Lee et al. [32] showed that the ansatz of Ott and Antonsen [17] could be applied to the time delayed case, but until this work no unified bifurcation analysis has been presented. Here we have presented such an analysis, allowing for the full description of the stability diagram for general parameter values which quantifies the transitions between incoherent, partially synchronized, and bistable states via a series of supercritical and subcritical Hopf bifurcations and a saddle node bifurcation of cycles. In particular, the transition from incoherence to partial synchronization occurs in one of two ways: (i) via a supercritical Hopf bifurcation in which case no bistability is observed, or (ii) via a subcritical Hopf bifurcation with a saddle node bifurcation of cycles in which case both the incoherent and partially synchronized states are stable for a range of coupling strengths. We note that the nature of bistability studied here is reminiscent of explosive synchronization observed in networks of coupled oscillators whose natural frequencies are correlated with the network structure [36, 37, 38].

In addition to the series of bifurcations that occur in the system, we also investigate the emergence of bistability. Specifically, this occurs at a codimension two point where the Hopf bifurcations collide with the saddle node bifurcation of cycles, which we express analytically. Moreover, this codimension two point also reveals a critical characteristic time delay that delineates the possibility for bistability. In particular, if the characteristic time delay is less than this critical value, then bistability cannot be observed in the system, regardless of the choices of the other system parameters. If the characteristic time delay is larger than this critical value, then bistability can be observed, provided that the other system parameters are appropriately tuned. This suggests that

the time delayed dynamics are only qualitatively different from the non-time delayed dynamics if the characteristic time delay in the system is sufficiently large.

The results presented in this work shed light on the general behaviors of collective behavior as they depend on time delay. In many real-world scenarios it is realistic to incorporate time delays between interacting dynamical units, provided that either (i) a signal takes some finite time to travel from one unit to another or (ii) a given dynamical unit takes some finite time to interpret signals from others. Our analysis illustrates that the presence of time delays induces multistability, provided that the time delay is large enough. In a broader context these results raise the question of whether multistability or possibly other nonlinear effects can be induced on the collective behaviors of ensembles of dynamical units of other types, for instance in the contexts of consensus or spreading processes. Moreover, if time delays do induce new nonlinear effects in their collective behaviors, an important question is whether or not these nonlinear effects, like those found here, arise only for sufficiently large time delays larger than some critical value.

References

- [1] A. Winfree. *The Geometry of Biological Time* (Springer, New York, 2001).
- [2] A. Pikovsky, M. Rosenblum, and J. Kurths. *Synchronization: A Universal Concept in Nonlinear Sciences* (Cambridge University Press, 2001).
- [3] J. Buck, Synchronous rhythmic flashing of fireflies. II., Q. Rev. Biol. **63**, 265 (1988).
- [4] S. H. Strogatz, Human sleep and circadian rhythms: a simple model based on two coupled oscillators, J. Math. Biol. **25**, 327 (1987).
- [5] L. Glass and M. C. Mackey. *From Clocks to Chaos: The Rhythms of Life* (Princeton University Press, 1988).
- [6] M. Rohen, A. Sorge, M. Timme, and D. Witthaut, Self-organized synchronization in decentralized power grids, Phys. Rev. Lett. **109**, 064101 (2012).
- [7] A. T. Winfree, Biological rhythms and the behavior of populations of coupled oscillators, J. Theor. Biol. **16**, 15 (1967).
- [8] Y. Kuramoto, in *International Symposium on Mathematical Problems in Theoretical Physics*, H. Araki, ed. *Lecture Notes in Physics* **39** (Springer, New York, 1975).
- [9] H. Sakaguchi, Cooperative phenomena in coupled oscillator systems under external fields, Prog. Theor. Phys. **79**, 39 (1988).
- [10] S. H. Strogatz and R. Mirollo, Stability of incoherence in a population of coupled oscillators, J. Stat. Phys. **63**, 613 (1991).
- [11] Y. Kuramoto. *Chemical Oscillations, Waves, and Turbulence* (Springer, New York, 1984).
- [12] J. D. Crawford, Amplitude expansions for instabilities in populations of globally-coupled oscillators, J. Stat. Phys. **74**, 1047 (1994).

- [13] S. Kim, S. H. Park, and C. S. Ryu, Multistability in coupled oscillator systems with time delay, *Phys. Rev. Lett.* **79**, 2911 (1997).
- [14] M. K. Stephen Yeung and S. H. Strogatz, Time delay in the Kuramoto model of coupled oscillators, *Phys. Rev. Lett.* **82**, 648 (1999).
- [15] M. Y. Choi, H. J. Kim, D. Kim, and H. Hong, Synchronization in a system of globally coupled oscillators with time delay, *Phys. Rev E*, **61**, 371 (2000).
- [16] E. Montbrió, D. Pazó, and J. Schmidt, Time delay in the Kuramoto model with bimodal frequency distribution, *Phys. Rev. E* **74**, 056201 (2006).
- [17] E. Ott and T. M. Antonsen, Low dimensional behavior of large systems of globally coupled oscillators, *Chaos* **18**, 037113 (2008).
- [18] E. Ott and T. M. Antonsen, Long time evolution of phase oscillator systems, *Chaos* **19**, 023117 (2009).
- [19] L. M. Childs and S. H. Strogatz, Stability diagram for the forces Kuramoto model, *Chaos* **18**, 043128 (2008).
- [20] E. A. Martens, E. Barreto, S. H. Strogatz, E. Ott, P. So, and T. M. Antonsen, Exact results for the Kuramoto model with a bimodal frequency distribution, *Phys. Rev. E* **79**, 026204 (2009).
- [21] D. Pazó and E. Montbrió, Existence of hysteresis in the Kuramoto model with bimodal frequency distributions, *Phys. Rev. E* **80**, 046215 (2009).
- [22] D. M. Abrams, R. Mirollo, S. H. Strogatz, and D. A. Wiley, Solvable model for chimera states of coupled oscillators, *Phys. Rev. Lett.* **101**, 084103 (2008).
- [23] E Barreto, B. Hunt, E. Ott, and P. So, Synchronization in networks of networks: The onset of coherent collective behavior in systems of interacting populations of heterogeneous oscillators, *Phys. Rev. E* **77**, 036107 (2008).
- [24] P. S. Skardal and J. G. Restrepo, Hierarchical synchrony of phase oscillators in modular networks, *Phys. Rev. E* **85**, 016208 (2012).
- [25] J. G. Restrepo and E. Ott, Mean-field theory of assortative networks of phase oscillators, *Europhys. Lett.* **107**, 60006 (2014).
- [26] P. S. Skardal, J. G. Restrepo, and E. Ott, Frequency assortativity can induce chaos in oscillator networks, *Phys. Rev. E* **91**, 060902(R) (2015).
- [27] D. Pazó and E. Montbrió, Low-dimensional dynamics of populations of pulse-coupled oscillators, *Phys. Rev. X* **4**, 011009 (2014).
- [28] T. Luke, E. Barreto, and P. So, Macroscopic complexity from an autonomous network of networks of theta neurons, *Front. Comput. Neurosci.* **8**, 145 (2014).
- [29] C. Laing, Derivation of a neural field model from a network of theta neurons, *Phys. Rev. E* **90**, 010901(R) (2014).

- [30] H. Hong and S. H. Strogatz, Kuramoto model of coupled oscillators with positive and negative coupling parameters: An example of conformist and contrarian oscillators, *Phys. Rev. Lett.* **106**, 054102 (2011).
- [31] P. S. Skardal, E. Ott, and J. G. Restrepo, Cluster synchronization in systems of coupled phase oscillators with higher-order coupling, *Phys. Rev. E* **84**, 036208 (2011).
- [32] W. S. Lee, E. Ott, and T. M. Antonsen, Large coupled oscillator systems with heterogeneous interaction delays, *Phys. Rev. Lett.* **103**, 044101 (2009).
- [33] C. R. Laing, Fronts and bumps in spatially extended Kuramoto networks, *Physica D* **240**, 1960 (2011).
- [34] W. S. Lee, J. G. restrepo, E. Ott, and T. M. Antonsen, Dynamics and pattern formation in large systems of spatially-coupled oscillators with finite response times, *Chaos* **21**, 023122 (2011).
- [35] P. S. Skardal, D. Taylor, and J. G. Restrepo, Complex macroscopic behavior in systems of phase oscillators with adaptive coupling, *Physica D* **267**, 27 (2014).
- [36] J. Gómez-Gardeñes, S. Gómez, A. Arenas, and Y. Moreno, Explosive synchronization transition in scale-free networks, *Phys. Rev. Lett.* **106**, 128701 (2011).
- [37] T. K. D. M. Peron and F. A. Rodrigues, Explosive synchronization enhanced by time-delayed coupling, *Phys. Rev. E* **86**, 016102 (2012).
- [38] P. S. Skardal and A. Arenas, Disorder induces explosive synchronization, *Phys. Rev. E* **89**, 062811 (2014).